ChemComm

Bimetallic Iron-Tin Catalyst for N_2 to NH_3 and a Silyldiazenido Model Intermediate

Journal:	*ChemComm*
Manuscript ID	CC-COM-07-2020-004563.R1
Article Type:	Communication

COMMUNICATION

Bimetallic Iron-Tin Catalyst for N_2 to NH_3 and a Silyldiazenido Model Intermediate

Received 00th January 20xx,
Accepted 00th January 20xx

DOI: 10.1039/x0xx00000x

Michael J. Dorantes,[a§] James T. Moore, [a§] Eckhard Bill, [b] Bernd Mienert,[b] and Connie C. Lu*[a]

A tin–supported iron catalyst produces 5.9 turnovers of NH_3 from N_2, using $[Ph_2NH]OTf$ as the acid and $CoCp^*_2$ as the reductant. Two redox states of the Fe(N_2) adduct and an Fe silyldiazenido complex were characterized by X–ray crystallography with NMR and Mössbauer spectroscopies. Density functional theory calculations reveal that the charge on the Sn center correlates strongly with both the polarization of the N_2 moiety and the charge on the distal N atom.

Conversion of dinitrogen into reduced feedstocks using well-defined transition-metal catalysts has steadily advanced since Schrock and Yandulov reported the Mo triamidoamine catalyst in 2003.[1] The development of other metal–based catalysts for N_2 fixation has led to a greater understanding of diverse mechanisms and increasingly high catalytic turnovers.[2] Notably, Nishibayashi and coworkers reported a Mo pincer catalyst capable of producing 4,350 equiv of NH_3 using $HOCH_2CH_2OH/SmI_2$ as a coupled proton and electron source.[3] However, these research developments are weighted primarily toward early transition metals. Comparatively, the number of late–transition metal catalysts are limited, including Fe–based catalysts (Figure 1).[4]

Here, we report an Fe catalyst that is largely inspired by Peters' nitrogen fixation catalyst, $P_3^BFe^+$, (P_3^B = tris(*o*–diisopropylphosphinophenyl)–borane).[4b,5] In comparison to other anchoring atoms such as C and Si, Peters and coworkers have concluded that the borane uniquely enhances the catalytic performance by conferring stability to the hydrazido intermediate, $FeNNH_2$.[6] Using a previously reported bimetallic Fe-Sn system,[7] we generated the N_2 adduct, $LSnFeN_2$ (**1**), where L is the double-decker ligand, $[N(o\text{–}(NCH_2P^iPr_2)C_6H_4)_3)]^{3-}$. Complex **1** mediates the catalytic reduction of N_2 to NH_3 with 5.9 turnovers. The properties of **1**, its reduced analogue, $K(THF)_3{\cdot}LSnFe(N_2)$ (**2**), and the N_2-functionalized diazenido complex, $LSnFeN_2SiMe_3$ (**3**), were characterized structurally, spectroscopically, and theoretically. To the best of our knowledge, this work provides the first examples of catalytic N_2 reduction that leverages a direct Fe–Sn interaction. Also, this study adds to the limited examples of Sn-supported first-row transition metal complexes.[8]

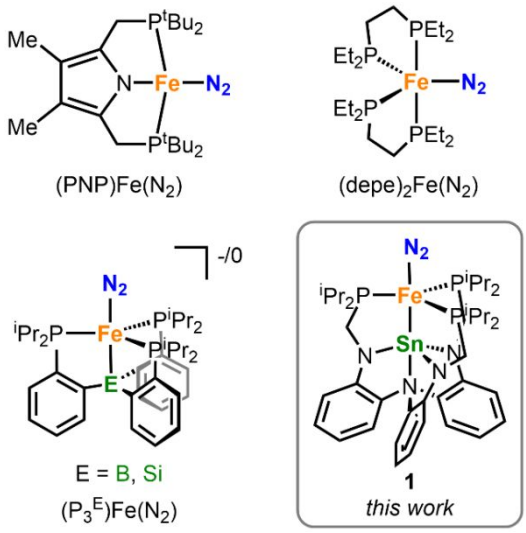

Fig. 1 Selected Fe–based catalysts for N_2 fixation.[4]

Addition of $FeBr_2$ to the metalloligand $[Li(THF)_3][LSn]$ in THF led to the previously reported bimetallic complex, LSnFeBr.[7] Crystallization of LSnFeBr by Et_2O diffusion into a concentrated benzene solution provided deep-red crystals in 68 % yield. Next, the one- and two-electron reductions of LSnFeBr in THF under an N_2 atmosphere were effected by adding 1.1 equiv and 2.2 equiv KC_8, respectively, whereupon the solution changed color from red to yellow orange and then to deep orange. The one-electron reduced species, $LSnFe(N_2)$ (**1**), is paramagnetic with an S = ½ ground state (μ_{eff} = 1.87 μ_B, Evans method). The N_2 ligand is bound in a terminal, end-on manner (vide infra). The N–N stretching frequency of 2011 cm^{-1} (IR, KBr pellet, ESI Fig. S11) indicates moderate activation of the N_2 unit that is comparable to other polyphosphine $Fe(N_2)$ complexes.[9] The doubly reduced

[a]*Department of Chemistry, University of Minnesota, 207 Pleasant Street SE, Minneapolis, Minnesota 55455-0431, United States. E-mail: clu@umn.edu*
[b]*Max Planck Institut für Chemische Energiekonversion, Stiftstraße 34-36, 45470 Mülheim an der Ruhr, Germany.*
§ co-first authors
† Electronic Supplementary Information (ESI) available: Experimental details for the synthesis, spectroscopic characterization, crystallographic data, catalysis data and DFT calculations. CCDC 2007833-2007836. For ESI, crystallographic data in CIF format, and DFT-optimized geometries in xyz format see DOI: 10.1039/x0xx00000x

species, K(THF)$_3$·LSnFe(N$_2$) (**2**), is diamagnetic and displays a single ^{31}P{^{1}H} NMR peak at 88.2 ppm (THF-d$_8$). A ^{119}Sn NMR quartet peak was observed at 511.6 ppm, which arises from the ^{119}Sn nucleus coupling to three equivalent ^{31}P nuclei (100%) through the Fe nucleus, with a $^2J_{Sn-P}$ value of 610 Hz (ESI Fig. S4). The ^{1}H{^{31}P} NMR spectrum with seven unique resonances is consistent with trigonal symmetry in solution (ESI Fig. S2). The N–N stretching frequency for the [2.2.2]cryptand derivative, K(crypt-222)[LSnFe(N$_2$)], of 1944 cm^{-1} (IR, KBr pellet, ESI Fig. S12), supports increased electron density at Fe, allowing for amplified backbonding into the N$_2$ π* orbitals.

Single-crystal X–ray diffraction studies were performed for **1** and **2** (see ESI). In both structures, the Fe center is trigonal bipyramidal with an end-on N$_2$ ligand in the axial position *trans* to the Sn center (Figure 2). The N–N bond elongates by 0.03 Å from 1.112(2) Å in **1** to 1.143(6) Å in **2** (*c.f.* free N$_2$ 1.10 Å, Table S2). The Fe–N$_2$ bond contracts by the same magnitude, consistent with increased Fe-to-N$_2$ π-backbonding in **2**. Notably, all the other bonds around Fe contracted upon reduction. In comparing **2** to **1**, the Fe–Sn and avg Fe–P bonds are shorter by 0.03 and 0.07 Å, respectively. As an aside, the Fe–Sn bond lengths (2.4470(3) in **1** and 2.4215(8) Å in **2**) are both smaller than the sum of their covalent radii (*c.f.* 2.59 Å), suggesting the presence of an Fe–Sn bonding interaction. Complex **2** crystallized as a 1-D coordination polymer, where the bridging K$^+$ ion is chelated by the ligand backbone of one molecule while binding the N$_2$ ligand of another. Because of a singularly short K–N$_{eq}$ interaction, one of the Sn–N$_{eq}$ bonds is significantly elongated in **2**, precluding a direct comparison of the Sn first-coordination shell between **1** and **2**.

In heterobimetallic complexes, the presence of intermetal covalent bond(s) can complicate the assignment of formal oxidation states of the individual metal centers. Adapting the Feltham–Enemark notation[10] to tally the total valence electrons of the bimetal unit, [11] the electronic configurations for LSnFeBr, **1**, and **2** are denoted as {FeSn}^{8}, {FeSn}^{9}, and {FeSn}^{10}. This redox triad was interrogated through an electrochemical study of **1** and **2**. The cyclic voltammograms (ESI Fig. S14 & S15) revealed a reversible one-electron redox event at $E_{1/2}$ = −1.89 V vs FeCp$_2^{+/0}$, which is assigned to the {FeSn}$^{9/10}$ redox couple, and an irreversible oxidation at E_{pa} ~ −0.76 V (0.4 M [^{n}Bu$_4$N][PF$_6$] in THF). For the latter oxidation, the irreversibility is likely due to N$_2$ dissociation from the cationic {FeSn}^{8} species.

Starting from the {FeSn}^{10} species **2**, N$_2$ functionalization was effected by using an electrophilic reagent in accord with literature precedent.[9c] Reaction of **2** with a slight excess of Me$_3$SiCl yielded the diazenido complex, LSnFeN$_2$SiMe$_3$ (**3**), as a lavender powder that is highly soluble in organic solvents ranging from pentane to THF. Structurally characterized Fe diazenido complexes that are derived from N$_2$ are still limited in the literature.[6c, 9c, 12] The N–N vibration at 1756 cm^{-1} (IR, KBr pellet, ESI Fig. S13) for **3** compares well with the reported values for Fe diazenido complexes (ESI Table S3).[9c, 12a] Complex **3** contains several NMR-active nuclei and was characterized by a suite of heteronuclear NMR spectroscopies (Figure 2). A downfield ^{31}P{^{1}H} NMR resonance at 101.3 ppm was observed with satellites arising from $^2J_{P-Sn}$ coupling to the ^{119}Sn (natural abundance: 7.7%) and ^{117}Sn (8.6%) nuclei of 561 and 538 Hz, respectively. In the ^{119}Sn NMR spectrum, a quartet was observed at 441.5 ppm, with a matching $^2J_{Sn-P}$ value of 559 Hz. Compared to **2**, **3** has a slightly lower $^2J_{Sn-P}$ value, which is consistent with the longer Fe–Sn bond in **3**. The ^{29}Si NMR resonance at –11.0 ppm falls well within the range of previously reported resonances for Fe silyldiazenido complexes[9c, 12a]

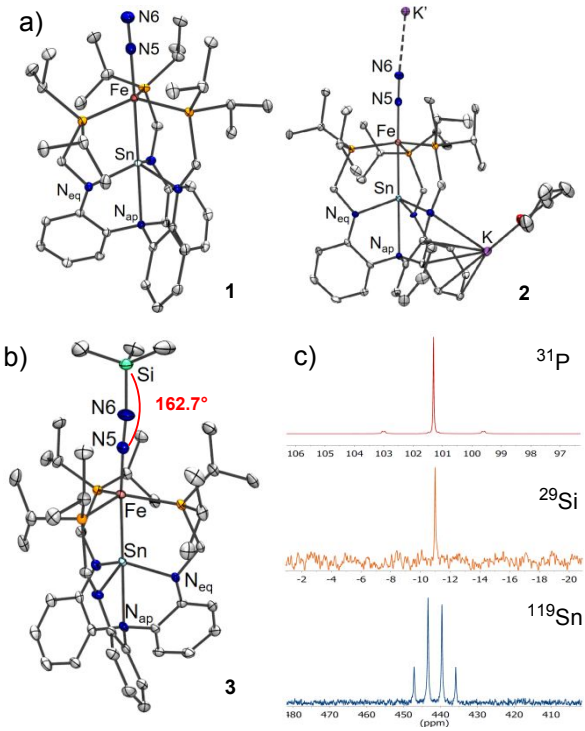

Fig. 2 a,b) Solid-state structures of **1**, **2**, and **3**. Thermal ellipsoids set at 50% probability with hydrogen atoms omitted. c) ^{31}P{^{1}H}, ^{29}Si, and ^{119}Sn NMR spectra of **3** in THF–d$_8$. (See ESI for full spectra.)

Single crystals of **3** were grown from a concentrated Et$_2$O solution stored at –30 °C for 48 h (Fig. 2). The structure shows that the N–N bond lengthened to 1.182(3) Å, which is intermediate between a double (1.25 Å) and triple (1.10 Å) N–N bond. The Fe–N bond contracted to 1.686(2) Å, which indicates multiple bond character.[13] The remaining bonds in the Fe first-coordination shell are expanded in **3** relative to **2**, where the avg Fe–P and Fe–Sn bond increases by 0.04 and 0.05 Å, respectively. The N–N–Si vector has a corresponding bond angle of 162.7(3)°, a value that is between linear and bent (~130°).[14] This bond angle is similar to that in (P$_3^{Si}$)Fe(N$_2$SiMe$_3$) (165.6°), but in sharp contrast to bent angles in [Fe(diphosphine)$_2$(N$_2$SiMe$_3$)][BAr$^F_4$] complexes (127°, 134°).[9c, 12a] Diazenido ligands, which are isoelectronic to nitrosyl ligands, are redox non-innocent, and hence, metal diazenido species can be described using two limiting resonance structures: M≐N=N–R and M–N≡N–R.[14] The former features a bent diazenido ligand (i.e. bent N–N–R angle) that is formally classified as a 3-electron, LX-donor; the latter is best described as a diazenium ligand, which akin to NO$^+$ is a cationic 2-electron L-donor. Collectively, the structural parameters in **3** support bonding that is in between these two resonance forms.

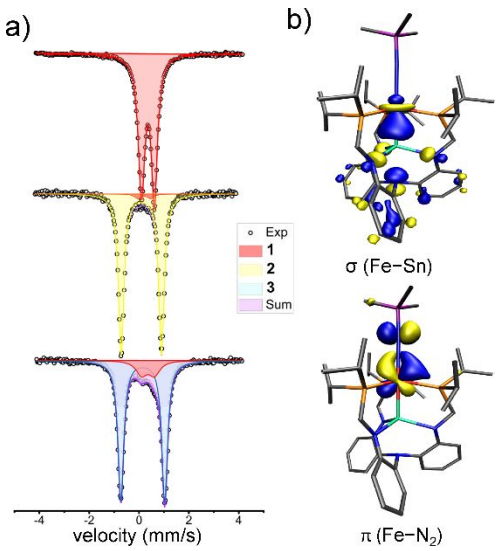

Fig. 3 a) Zero–field ^{57}Fe Mössbauer spectra recorded at 80 K. Experimental data is indicated by the dotted points. In samples of **2** and **3**, $LSnFeN_2$ (**1**) is present as an impurity at 3% and 14%, respectively. Tabulated parameters can be found in Table S4. **b)** DFT-calculated MOs of **3** showing the Fe-Sn σ-bond and the enhanced Fe–N_2 π-backbonding upon silylation.

Solid samples of **1**, **2**, and **3** were subjected to zero–field ^{57}Fe Mössbauer spectroscopy at 80 K. Each spectrum showed a relatively clean quadrupole doublet (Fig. 3a, Fig. S17 and Table S4). The isomer shift (δ) steadily decreases from **1** to **2** to **3**: 0.47, 0.35, and 0.26 mm/s, respectively. The observed decrease in δ upon reduction is typical for low-valent Fe systems.[15] The lowering of δ has been attributed to the increase in the Fe 4*s* population that arises from greater Fe-to-L π–backbonding, or shorter, more covalent Fe-L bonds.[15a, 16] In this series, the only bond that consistently contracts is the Fe–N bond (whether the ligand is N_2 or N_2SiMe_3), which decreases from 1.793 Å in **1** to 1.762 Å in **2**, and then to 1.686 Å in **3**. The quadrupole splitting ($|\Delta E_Q|$) increases from 0.52 mm/s in **1** to 1.62 mm/s in **2**, but only slightly increases to 1.76 mm/s in **3**. The trends in both δ and $|\Delta E_Q|$ match well to those reported for $[(P_3^{Si})Fe(N_2)]^{0/-}$ and $(P_3^{Si})Fe(N_2SiMe_3)$ (Table S4).[9c, 17] The δ values for **2** and **3** are different (Δ = 0.11 mm/s), whereas the $|\Delta E_Q|$ values are similar. Hence, it remains unclear whether the configuration of $\{SnFe(N_2R)\}^{10}$ in **3** would be best described as an $\{FeSn\}^{10}$ unit that π–backbonds into a silyldiazenium(1+) moiety or an $\{FeSn\}^8$ unit with a π–donating diazenido(2-) ligand.

Density functional theory (DFT) calculations (M06–L, see ESI for computational details) were also performed to probe the electronic structures of **1**–**3**. Overall, there is good agreement between the computed and experimental geometries (ESI Table S5). The resulting MO diagrams for **1**–**3** all show a covalent Fe–Sn σ-bond, where the Sn (5p_z, 6*s*) and Fe (3d_z^2) contributions are almost equal (Fig. 3b, ESI Fig. S18-S20). The ground-state configurations of **1** and **2** are consistent with $(\sigma_{Fe-Sn})^2$(Fe d_{xz}, d_{yz})^4(Fe d_{xy}, $d_{x^2-y^2}$)^n$(\sigma^*_{Fe-Sn})^0$, where *n* is 3 and 4, respectively. The MO diagram for **3** also shows highly covalent π-bonds between Fe and N_2SiR_3, and is consistent with the ground-state configuration: $(\sigma_{Fe-Sn})^2(\pi_{Fe-N2})^4$(Fe-$d_{xy}$, $d_{x^2-y^2}$)^4$(\pi^*_{Fe-N2})^0(\sigma^*_{Fe-Sn})^0$.

To elucidate the bonding in **1**–**3**, the Fe–N and N–N bond orders were analyzed using the density derived electrostatic and chemical (DDEC6) method.[18] This analysis revealed a gradual increase in the Fe–N bond order from **1** to **2** to **3**: 1.13, 1.20, and 1.50, respectively (ESI Fig. S21). Simultaneously, the N–N bond order decreases from **1** to **2** to **3**: 2.58, 2.56, and 2.18, respectively. Indeed, coordination of the $SiMe_3^+$ group results in a more polarized and weakened N–N bond, as reflected by the increased negative charge on the distal N-atom in **3** (−0.37) compared to **1** (−0.15) and **2** (−0.24) (ESI Table S9). Similar trends were observed upon the coordination of Lewis acidic boranes to the distal N of $Fe(depe)_2(N_2)$, culminating in the selective protonation at the distal N site due to its enhanced negative charge.[12b] In **1**-**3**, the charge of the distal N as well as the charge difference between the N atoms were found to correlate best with the charge of Sn (R^2_{adj} = 0.997 and 0.988, respectively, Fig. S23-S24). These strong correlations suggest that the identity of the atom *trans* to the N_2 unit may have a substantial effect on the distal N's nucleophilicity, which would likely govern how readily the N_2 unit can undergo further functionalization.

Next, we investigated the catalytic performance of **1**–**3** in reducing N_2 to NH_3. Using similar conditions to those developed by Peters and coworkers,[4b] the catalyst (2.3 μmol), $[Ph_2NH_2]OTf$ (108 equiv), $CoCp^*_2$ (54 equiv), and Et_2O were sealed in a vessel while under 1 atm N_2 at –196 °C, and then stirred at –78 °C for 3 h. The $Ph_2NH_2^+$ acid and the $CoCp^*_2$ reductant are proposed to initially form the protonated metallocene, Co(η^4-Cp*H)(Cp*), which mediates proton–coupled electron transfer during N_2 reduction.[5] Table 1 summarizes the results of the catalytic runs, which were performed in triplicate (ESI Table S10). Catalyst **1** generated 5.9(5) turnovers of NH_3 (33% yield, entry 1). Moreover, catalytic activity was retained in the presence of $Hg_{(s)}$ (entry 2), supporting an active species that is homogeneous. In comparison, the $P_3^BFe^+$ catalyst produced 12.8 turnovers of NH_3 in a single catalytic run and reached 84 NH_3 turnovers after 3 consecutive runs (entries 5 and 6).[5] For NH_3 production under these specific conditions, **1** is half-fold as active as $P_3^BFe^+$ in a single catalytic run, and outperforms both $P_3^{Si}Fe(N_2)$[5] and $Fe(depe)_2(N_2)$[12a] by five-fold (entries 7 and 8). We note that other Fe catalysts require harsher reagents such as $H(Et_2O)B(Ar^F)_4$ and KC_8 to mediate N_2 to NH_3.[4c-e, 19a, 19b]

The N_2 reduction reaction, however, was rendered substoichiometric when **2** was employed as the catalyst (entry 3). Presumably, this poor activity is caused by the low solubility of **2** in Et_2O. On the other hand, catalyst **3** gave comparable turnovers (entry 4) as **1**, supporting the ability of a metal silyldiazenido species to enter the N_2 reduction cycle. Because metal silyldiazenido species are proposed as intermediates in catalytic N_2 silylation, we also tested **3** for N_2 silylation using Me_3SiCl and KC_8 as the added reagents. Disappointingly, **3** only generated 1.2 equiv of $N(SiMe_3)_3$, which is relatively poor compared to other reported systems.[2b] While we do not yet understand the stark activity difference of **3** in regards to N_2 fixation versus N_2 silylation, this disparity has also been noted by others.[20]

Table 1. Results of catalytic reduction of dinitrogen to ammonia using Fe–Sn complexes (**1**–**3**) and comparisons to known Fe catalysts.

N_2 + $CoCp^*_2$ + $[Ph_2NH_2]OTf$ —*Fe catalyst*, Et_2O, -78 °C, 3 h→ NH_3

x equiv *y* equiv

entry	catalyst	*x* (equiv)	*y* (equiv)	NH_3 turnovers	yield [a] (%)	ref.
1	**1**	54	108	5.9(5)	33	–
2	**1** + $Hg_{(s)}$ [b]	54	108	5.2(8)	29	–
3	**2**	54	108	0.8(5)	5	–
4	**3**	54	108	4.6(2)	26	–
5	$P_3^BFe^+$	54	108	12.8(5)	72	4b
6	$P_3^BFe^+$	162 × 3[c]	322 × 3[c]	84(8)	52	4b
7	$P_3^{Si}Fe(N_2)$	54	108	1.2(1)	7	4b
8	$(depe)_2Fe(N_2)$	54	108	1.1(2)[d]	6	4g

[a]Yield is based on the reductant. [b]200 equiv Hg was added to the reaction vessel before the start of catalysis. [c]In each of the 3 cycles, the reaction was cooled to –196 °C to replenish the reagents and solvent. [d]$(depe)_2Fe(N_2)$ is selective for hydrazine with 8.9(1) equiv N_2H_4 in addition to 1.1(2) equiv NH_3.

A family of Fe-Sn bimetallic complexes has enabled the characterization and comparison of a series of nitrogen fixation catalysts, capable of generating ammonia in up to 5.9 equivalents. Experimental and computational results together show a clear and comparable trend of increased N_2 activation (evidenced by decreased N_2 bond order, stretching frequency, and increased negative charge on the distal nitrogen) upon reduction from **1** to **2**, and even more so in the silylation of **2** to **3**. For all of these complexes, a direct Fe-Sn covalent interaction was present, and a linear trend was found between the charge on Sn and the charge on the distal nitrogen in the N_2 moiety. This points to another potential impact of the supporting atom *trans* to the N_2 moiety on N_2 functionalization. Indeed, the effect of ligands *trans* to the N_2 unit of metal complexes has long been proposed to impact the overall efficacy of N_2 functionalization.[21] Under the same catalytic conditions, the Fe-Sn bimetallic catalyst compares well with Peters' Fe-E systems, outperforming E = Si and C, but less active than E = B. These type of comparisons lend additional understanding into the factors that generate active Fe-E catalysts. Additional studies with different supporting atoms and further functionalization of the presented complexes are currently underway.

The authors thank the NSF (CHE-1800110) for support and Dr. Victor G. Young, Jr. (CHE-1229400) for X-ray crystallography.

Notes and references

1. D. V. Yandulov and R. R. Schrock, *Science*, 2003, **301**, 76-78.
2. (a) D. Singh, W. R. Buratto, J. F. Torres and L. J. Murray, *Chem. Rev.*, 2020, **120**, 5517-5581; (b) S. Kim, F. Loose and P. J. Chirik, *Chem. Rev.*, 2020, **120**, 5637–5681; (c) M. J. Chalkley, M. W. Drover and J. C. Peters, *Chem. Rev.*, 2020, **120**, 5582–5636; (d) K. C. Macleod and P. L. Holland, *Nat. Chem.*, 2013, **5**, 559-565; (e) R. J. Burford and M. D. Fryzuk, *Nat. Rev. Chem.*, 2017, **1**, 0026.
3. Y. Ashida, K. Arashiba, K. Nakajima and Y. Nishibayashi, *Nature*, 2019, **568**, 536-540.
4. (a) J. Higuchi, S. Kuriyama, A. Eizawa, K. Arashiba, K. Nakajima and Y. Nishibayashi, *Dalton Trans.*, 2018, **47**, 1117-1121; (b) M. J. Chalkley, T. J. Del Castillo, B. D. Matson and J. C. Peters, *J. Am. Chem. Soc.*, 2018, **140**, 6122-6129; (c) R. Imayoshi, K. Nakajima, J. Takaya, N. Iwasawa and Y. Nishibayashi, *Eur. J. Inorg. Chem.*, 2017, **2017**, 3769-3778; (d) S. Kuriyama, K. Arashiba, K. Nakajima, Y. Matsuo, H. Tanaka, K. Ishii, K. Yoshizawa and Y. Nishibayashi, *Nat. Commun.*, 2016, **7**, 12181; (e) S. E. Creutz and J. C. Peters, *J. Am. Chem. Soc.*, 2014, **136**, 1105-1115; (f) Y. Sekiguchi, S. Kuriyama, A. Eizawa, K. Arashiba, K. Nakajima and Y. Nishibayashi, *Chem. Comm.*, 2017, **53**, 12040-12043; (g) P. J. Hill, L. R. Doyle, A. D. Crawford, W. K. Myers and A. E. Ashley, *J. Am. Chem. Soc.*, 2016, **138**, 13521-13524; (h) J. S. Anderson, J. Rittle and J. C. Peters, *Nature*, 2013, **501**, 84-87.
5. M. J. Chalkley, T. J. Del Castillo, B. D. Matson, J. P. Roddy and J. C. Peters, *ACS Cent. Sci.*, 2017, **3**, 217-223.
6. (a) B. D. Matson and J. C. Peters, *ACS Catal.*, 2018, **8**, 1448-1455; (b) M. M. Deegan and J. C. Peters, *Chem. Sci.*, 2018, **9**, 6264-6270; (c) J. Rittle and J. C. Peters, *J. Am. Chem. Soc.*, 2016, **138**, 4243-4248.
7. S. C. Coste, B. Vlaisavljevich and D. E. Freedman, *Inorg. Chem.*, 2017, **56**, 8195-8202.
8. D. Das, S. S. Mohapatra and S. Roy, *Chem. Soc. Rev.*, 2015, **44**, 3666-3690.
9. (a) J. S. Anderson, M. E. Moret and J. C. Peters, *J. Am. Chem. Soc.*, 2013, **135**, 534-537; (b) L. R. Doyle, P. J. Hill, G. G. Wildgoose and A. E. Ashley, *Dalton Trans.*, 2016, **45**, 7550-7554; (c) Y. Lee, N. P. Mankad and J. C. Peters, *Nat. Chem.*, 2010, **2**, 558-565; (d) M. E. Moret and J. C. Peters, *J. Am. Chem. Soc.*, 2011, **133**, 18118-18121.
10. J. H. Enemark and R. D. Feltham, *Coord. Chem. Rev.*, 1974, **13**, 339-406.
11. (a) B. Wu, M. J. Wilding, S. Kuppuswamy, M. W. Bezpalko, B. M. Foxman and C. M. Thomas, *Inorg. Chem.*, 2016, **55**, 12137-12148; (b) R. J. Eisenhart, P. A. Rudd, N. Planas, D. W. Boyce, R. K. Carlson, W. B. Tolman, E. Bill, L. Gagliardi and C. C. Lu, *Inorg. Chem.*, 2015, **54**, 7579-7592.
12. (a) A. D. Piascik, P. J. Hill, A. D. Crawford, L. R. Doyle, J. C. Green and A. E. Ashley, *Chem. Comm.*, 2017, **53**, 7657-7660; (b) J. B. Geri, J. P. Shanahan and N. K. Szymczak, *J. Am. Chem. Soc.*, 2017, **139**, 5952-5956.
13. P. L. Holland, *Dalton Trans.*, 2010, **39**, 5415-5425.
14. J. R. Dilworth, *Coord. Chem. Rev.*, 2017, **330**, 53-94.
15. (a) F. Neese, *Inorg. Chim. Acta*, 2002, **337**, 181-192; (b) P. B. Gutlich, E.; Trautwein, A. X., *Springer*.
16. J. T. Moore, S. Chatterjee, M. Tarrago, L. J. Clouston, S. Sproules, E. Bill, V. Bernales, L. Gagliardi, S. Ye, K. M. Lancaster and C. C. Lu, *Inorg. Chem.*, 2019, **58**, 6199-6214.
17. P. A. Rudd, N. Planas, E. Bill, L. Gagliardi and C. C. Lu, *Eur. J. Inorg. Chem.*, 2013, **2013**, 3898-3906.
18. (a) N. G. Limas and T. A. Manz, *RSC Advances*, 2018, **8**, 2678-2707; (b) T. A. Manz, *RSC Adv.*, 2017, **7**, 45552-45581.
19. (a) Y. Nishibayashi, *Dalton Trans.*, 2018, **47**, 11290-11297; (b) T. J. Del Castillo, N. B. Thompson and J. C. Peters, *J. Am. Chem. Soc.*, 2016, **138**, 5341-5350.
20. (a) A. D. Piascik, R. Li, H. J. Wilkinson, J. C. Green and A. E. Ashley, *J. Am. Chem. Soc.*, 2018, **140**, 10691–10694; (b) G. Ung and J. C. Peters, *Angew. Chem. Int. Ed. Engl.*, 2015, **54**, 532-535; (c) A. J. Kendall, S. I. Johnson, R. M. Bullock and M. T. Mock, *J. Am. Chem. Soc.*, 2018, **140**, 2528-2536.
21. J. Chatt, A. J. Pearman, R. L. Richards, *Nature*, 1975, **253**, 39-40.